

## Double point source W-phase inversion: Real-time implementation and automated model selection



Jennifer L. Nealy <sup>a,b,\*</sup>, Gavin P. Hayes <sup>a</sup>

<sup>a</sup> U.S. Geological Survey, National Earthquake Information Center, Golden, CO, United States

<sup>b</sup> Colorado School of Mines, Golden, CO, United States

### ARTICLE INFO

**Article history:**

Received 16 July 2015

Received in revised form 11 September 2015

Accepted 13 September 2015

Available online 28 September 2015

**Keywords:**

Earthquake source observations

Surface waves and free oscillations

Wave propagation

Early warning

### ABSTRACT

Rapid and accurate characterization of an earthquake source is an extremely important and ever evolving field of research. Within this field, source inversion of the W-phase has recently been shown to be an effective technique, which can be efficiently implemented in real-time. An extension to the W-phase source inversion is presented in which two point sources are derived to better characterize complex earthquakes. A single source inversion followed by a double point source inversion with centroid locations fixed at the single source solution location can be efficiently run as part of earthquake monitoring network operational procedures. In order to determine the most appropriate solution, i.e., whether an earthquake is most appropriately described by a single source or a double source, an Akaike information criterion (AIC) test is performed. Analyses of all earthquakes of magnitude 7.5 and greater occurring since January 2000 were performed with extended analyses of the September 29, 2009 magnitude 8.1 Samoa earthquake and the April 19, 2014 magnitude 7.5 Papua New Guinea earthquake. The AIC test is shown to be able to accurately select the most appropriate model and the selected W-phase inversion is shown to yield reliable solutions that match published analyses of the same events.

Published by Elsevier B.V.

### 1. Introduction

The W-phase is a long period (up to 1000 s) phase of a seismic source that arrives between the P- and S-wave phases. Kanamori and Rivera (2008) were the first to use the W-phase in an accurate method for assessing source properties of great earthquakes, i.e., earthquakes with magnitudes of at least  $M_w$  8.0. More recently, source inversion of the W-phase has been extended to earthquakes with much lower magnitudes, and has been implemented in real-time by the National Earthquake Information Center (NEIC) of the U.S. Geological Survey (USGS), the Pacific Tsunami Warning Center (PTWC) of the National Oceanic and Atmospheric Administration (NOAA), and the Institut de Physique du Globe de Strasbourg (IPGS) (Hayes et al., 2009; Duputel et al., 2011). Although multiple authors (Duputel et al., 2012; Lay et al., 2013b) have demonstrated that multiple point source inversion using the W-phase is able to obtain accurate representations of events, the possible real-time applicability of a multiple source W-phase inversion has not been

explored. Here the W-phase source inversion is extended from the original approach that parameterized all earthquakes as point sources, to allow for a two point source solution. Fixing the centroid locations of the two sub-events and performing a grid search for the corresponding time delays can quickly obtain an accurate representation of a complex event. Once solutions have been found using both the traditional single source and the new double source W-phase inversions, an AIC test is performed to select the model that best represents the recorded data. Here we assess the performance of the double point source approach and show that not only are accurate results obtained in near-real-time but also the AIC test can be successfully used to select the best model.

### 2. Double point source W-phase methods

The double point source W-phase inversion involves four main stages. In the first stage, a single point source W-phase inversion is performed using the NEIC Preliminary Determinations of Epicenters (PDE) hypocenter. An initial magnitude estimate, obtained from either NEIC preliminary evaluations or from a NOAA tsunami warning center, is used to establish the appropriate filter; see Duputel et al. (2012b) and Table 1. The W-phase inversion for a single point source can be formulated as,

\* Corresponding author at: USGS NEIC, 1711 Illinois Street, Golden, CO 80401, United States

E-mail address: jnealy@usgs.gov (J.L. Nealy).

**Table 1**

Corner frequencies used for Butterworth bandpass filtering in the W-phase inversions. Corner frequencies are selected based on initial magnitude estimates.

Magnitude range ( $M_w$ )	Low corner (Hz) (s)	High corner (Hz) (s)
$M_w \geq 8.0$	0.001(1000 s)	0.005(200 s)
$8.0 > M_w \geq 7.5$	0.002(500 s)	0.0067(150 s)
$7.5 > M_w \geq 7.0$	0.002(500 s)	0.0083(120 s)
$7.0 > M_w \geq 6.5$	0.0025(400 s)	0.01(100 s)
$6.5 > M_w$	0.0067(150 s)	0.02(50 s)

$$\begin{bmatrix} u_1^{1,1} & u_1^{2,2} & \dots & u_1^{2,3} \\ u_2^{1,1} & u_2^{2,2} & \dots & u_2^{2,3} \\ \vdots & \vdots & \dots & \vdots \\ u_N^{1,1} & u_N^{2,2} & \dots & u_N^{2,3} \end{bmatrix} \begin{bmatrix} M_{11} \\ M_{22} \\ M_{33} \\ M_{12} \\ M_{13} \\ M_{23} \end{bmatrix} = \begin{bmatrix} d_1 \\ d_2 \\ \vdots \\ d_N \end{bmatrix}, \quad (1)$$

where  $M_{ij}$  is element  $i-j$  of the source deviatoric moment tensor,  $u_k^{ij}$  is the displacement at station  $k$  computed for a moment tensor with only  $M_{ij} = 1$  (i.e., the Green's functions), and  $d_k$  is the observed W-phase at station  $k$ . The inversion is performed using the least-squares technique. For more information on the details of the single source W-phase inversion, we refer you to Kanamori and Rivera (2008) and Hayes et al. (2009).

Once the single source solution has been obtained, the double point source W-phase inversion is performed using the centroid parameters of the single source inversion as a starting point. The centroid locations of both sub-events being considered in the double point source inversion are fixed at the centroid location found for the single source solution. Since centroid locations are derived using a least squares grid search approach, fixing the centroid locations greatly speeds up the run time of the inversion while still providing an accurate characterization of the two sub-events. In the third stage, a grid search is applied to find the time shift pair that minimizes the root mean square (RMS) error of the waveform misfit. During this step, both the time delays and the half-durations of the two sub-events are found within the grid search. While performing the grid search, a time delay and half-duration pair is only considered if applying the pair results in the first sub-event ending after the second sub-event begins and prior to the end of the second sub-event, and the second sub-event beginning after the first sub-event begins. Additionally, the half-durations are constrained based on the magnitude of the single source solution so that the half-durations selected for the two sub-events cannot exceed the half-duration of the single source solution and cannot be smaller than the half-duration of a  $M_w$  7.0 event. The half-durations are constrained in such a manner since the two sub-events combined should be equivalent to the single source solution and, since only events of  $M_w$  7.5 and greater are considered here, the two sub-events are not expected to have magnitudes much smaller than  $M_w$  7.0. The reference half-duration formula given by Duputel et al. (2013) was used to calculate the maximum and minimum half-durations. If two time delay and half-duration pairs are found with the same minimum RMS, the solution with the earlier time delays is selected.

A second inversion is then performed using the optimized time shift pair. The final stage compares the single source model and the double point source model using Akaike's method to determine the most appropriate model for the event (Akaike, 1972). The AIC test uses the number of degrees of freedom of each model along with their errors to evaluate the relative fit of each solution. Since we are comparing two models, we are interested in the difference between the AIC values of the models, which is given by,

$$\Delta\text{AIC} = N \times \ln \left( \frac{\text{SS2}}{\text{SS1}} \right) + 2\Delta\text{df},$$

where  $N$  is the length of the data,  $\text{SS1}$  is the sum-of-squares error for the single source inversion,  $\text{SS2}$  is the sum-of-squares error for the double source inversion, and  $\Delta\text{df}$  is the difference in degrees of freedom between the two models. In this case, since a deviatoric moment tensor is used, the single source inversion has 5 degrees of freedom and the double source inversion has 10 degrees of freedom. If  $\Delta\text{AIC}$  is a negative value, the double source model should be selected, otherwise the single source model is the better choice.

An additional benefit of using the difference between AIC values is the ability to easily compute the likelihood of a model for the given data. For each event, the Akaike weight for the double source model can be calculated as

$$w_{ds} = \frac{e^{-0.5\Delta\text{AIC}}}{(e^{-0.5\Delta\text{AIC}} + e^{-0.5 \times 0})}.$$

The Akaike weight for the single source model can be written in a similar manner as

$$w_{ss} = \frac{e^{-0.5 \times 0}}{(e^{-0.5\Delta\text{AIC}} + e^{-0.5 \times 0})}.$$

The weights, which sum to one, can be interpreted as the estimated probability that either the single or double source model is better. For example, if  $w_{ds} = 0.93$  and  $w_{ss} = 0.07$  the double source model is clearly the better representation of the event under consideration. For more information on Akaike's method or Akaike weights, we refer you to Akaike (1972), Akaike (1974), GraphPad (1994–2014), Burnham and Anderson (1998), and Canham (2013).

When a double point source inversion is performed, two sub-events are being inverted simultaneously. The W-phase inversion for a two point source event can therefore be formulated as an extended version of Eq. (1),

$$\begin{bmatrix} u_{1,1}^{1,1} & \dots & u_{1,N}^{1,1} & u_{2,1}^{1,1} & \dots & u_{2,N}^{1,1} \\ \vdots & \dots & \vdots & \vdots & \dots & \vdots \\ u_{1,1}^{2,1} & \dots & u_{1,N}^{2,1} & u_{2,1}^{2,1} & \dots & u_{2,N}^{2,1} \end{bmatrix} \begin{bmatrix} M_{11}^1 \\ M_{22}^1 \\ M_{33}^1 \\ M_{12}^1 \\ M_{13}^1 \\ M_{23}^1 \\ M_{11}^2 \\ M_{22}^2 \\ M_{33}^2 \\ M_{12}^2 \\ M_{13}^2 \\ M_{23}^2 \end{bmatrix} = \begin{bmatrix} d_1 \\ d_2 \\ \vdots \\ d_N \end{bmatrix}.$$

Here,  $M_{ij}^1$  is element  $i-j$  of the source deviatoric moment tensor for the first event and  $M_{ij}^2$  is element  $i-j$  of the source deviatoric moment tensor for the second event. Similarly,  $u_{1,k}^{ij}$  is the displacement at station  $k$  computed for a moment tensor with only  $M_{ij}^1 = 1$  while  $u_{2,k}^{ij}$  is the displacement at station  $k$  computed for a moment tensor with only  $M_{ij}^2 = 1$ . The observed W-phase at station  $k$  is still given by  $d_k$ , being a superposition of the two sub-events. As in the single point source case, the least-squares technique is used to perform the inversion.

If the double point source model is selected by the AIC test, an extended double point source W-phase inversion can be run to find the optimized centroid locations for the two sub-events. In order to find the centroid locations another grid search would be applied following the inversion using the optimized time shift pair. The centroid grid search performs a preliminary depth grid search

allowing the depths of both events to vary. Once a depth pair is selected, a grid search to find the optimal horizontal location (longitude, latitude) of the two sub-events is performed. Within the horizontal search the depths of the events are fixed at the optimal depths selected in the previous iteration. A final inversion using the optimized time shift pair and centroid locations yields the ultimate solution. The results shown here use fixed centroid positions when running the double point source model unless otherwise specified.

### 3. Results

In this section we present the results of applying the protocol previously defined, i.e., performing a single source inversion followed by a double point source inversion and AIC test, to earthquakes since January 1, 2000 with magnitudes of 7.5 or greater. The global centroid moment tensor (gCMT) solutions of the events selected for testing are shown in Fig. 1, plotted at their respective hypocenter locations and colored according to centroid depth (Ekström et al., 2012). The centroid moment tensor (CMT) solutions and magnitudes derived for these events using the protocol introduced in this paper are listed in Tables 2 and S1. The table lists the event name, the date the event occurred and the inversion type selected (single vs double source) along with the derived magnitudes and CMT solutions. The inversion type listed is the model selected by the AIC test. If a double point source model was selected, the magnitudes and focal mechanisms of both events are shown, in the order in which they occurred.

We anticipated that very few events would be classified as complex—i.e., as double source solutions. This expectation is validated by the results in Table 2, since the majority of events were classified as single source events. Overall, 83% of the 81 events considered here were classified as single sources using the AIC test. Of the 17% of events classified as double sources, seven earthquakes had been previously found to be multiple point sources (2000 Enggano, 2002 Central Alaska, 2004 Sumatra, 2008 Sichuan, 2009 Samoa Islands, 2012

Sumatra, 2013 Awaran), two earthquakes had been previously modeled only as single sources (2012 Haida Gwaii, 2007 Kuril), and five earthquakes had not been previously studied in-depth (2001 Gujarat, 2002 Papua, 2005 New Ireland, 2009 Andaman, 2014 Kirakira) (<http://earthquake.usgs.gov/eqcenter/eqinthenevents/2002/uslblb/reports/index.php>, 2002; [http://earthquake.usgs.gov/earthquakes/eventpage/usp000be54#scientific\\_finitefault](http://earthquake.usgs.gov/earthquakes/eventpage/usp000be54#scientific_finitefault), 2002; Abercrombie et al., 2003; Tsai et al., 2005; [http://earthquake.usgs.gov/earthquakes/eventpage/usp000h05x#scientific\\_finitefault](http://earthquake.usgs.gov/earthquakes/eventpage/usp000h05x#scientific_finitefault), 2009; Lay et al., 2010a,b; Nakamura et al., 2010; Gahalaut, 2012; [http://earthquake.usgs.gov/earthquakes/eventpage/usb000jyiv#scientific\\_finitefault](http://earthquake.usgs.gov/earthquakes/eventpage/usb000jyiv#scientific_finitefault), 2013; Zinke et al., 2014; Jolivet et al., 2014). There were also four single source solutions that had been found to be multiple point source events previously (2000 Wharton Basin, 2007 Peru, 2013 Scotia Sea, 2013 Sea of Okhotsk) (Robinson et al., 2001; Lay et al., 2010; Ye et al., 2014; Chen et al., 2014).

The magnitudes and CMTs for all of the single source solutions are in agreement with those found by the USGS and the gCMT group, with 62 of the 68 events having a magnitude within .1 of the W-phase inversion solution found in the USGS Comprehensive Catalog (ComCat). The magnitudes for the double source solutions are either in agreement with published literature, when such research has been performed, or sum to a moment similar to that given by the USGS and the gCMT group. In order to provide a more in-depth analysis of the technique presented in this paper, in the following section we describe full results of our procedure for two of the events in Table S1; the September 29, 2009 Samoa earthquake and the April 19, 2014 Panguna earthquake.

#### 3.1. Double source model – 2009 Samoa great earthquake

The 2009 Samoa great earthquake was found to be a double source event using the presented technique and has been previously identified as a multiple source event by other authors (Lay et al., 2010b; Beavan et al., 2010). In order to provide a full description of the two point source inversion procedure, the results

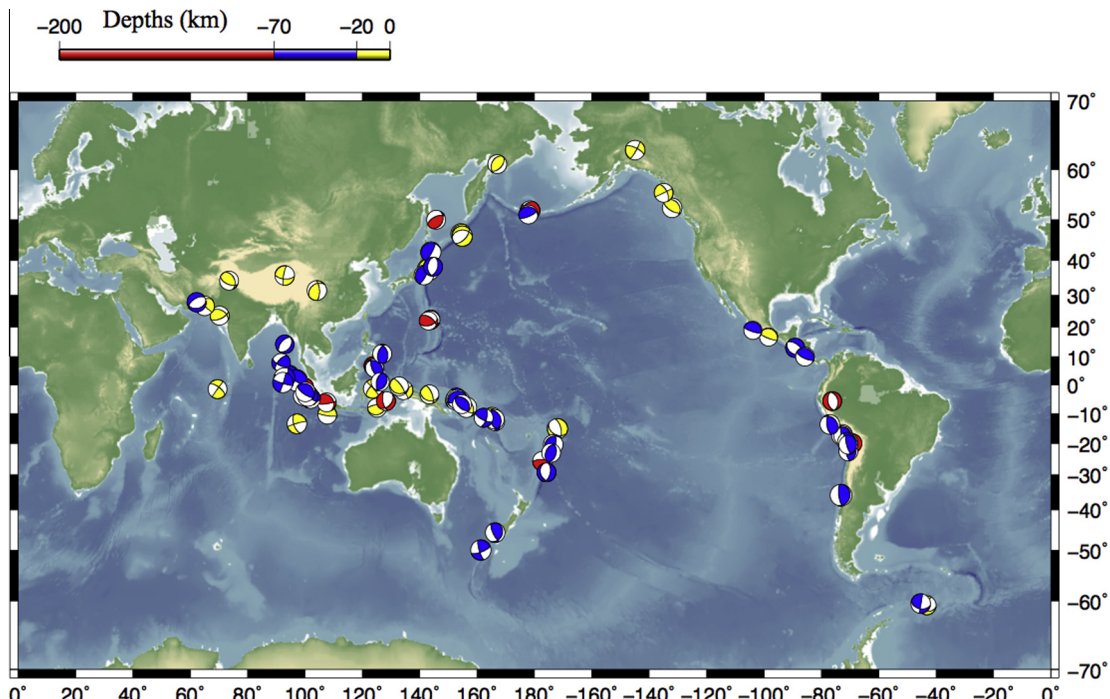


**Fig. 1.** Map of the world showing all M7.5+ earthquakes that have occurred since January 1, 2000. The events are represented by the corresponding global centroid moment tensor (GCMT) solution (Dziewonski et al., 1981; Ekström et al., 2012). The CMTs are colored according to the centroid depth of the event.

of the inversion, the results of all grid searches performed, and a comparison of waveforms are presented here. The W-phase solutions found using the double source inversion are shown in the inset of Fig. 2a. These CMTs were derived using a fixed centroid location corresponding to the single source solution. The W-phase double point source inversion infers a normal faulting sub-event followed by a thrust faulting sub-event. Both events are consistent with the results of previous studies of this complex earthquake (Lay et al., 2010b; Beavan et al., 2010).

Prior to finding the two solutions shown in Fig. 2b, a single source solution was derived. The CMT of the best single source solution is shown in Fig. 3a alongside a cross section of the inferred, single source slip distribution derived by the NEIC in the hours after the earthquake ([http://earthquake.usgs.gov/earthquakes/eqintheneWS/2009/us2009mdbi/finite\\_fault.php](http://earthquake.usgs.gov/earthquakes/eqintheneWS/2009/us2009mdbi/finite_fault.php), 2009). This event was inferred to have a large amount of slip surrounding the hypocenter with significant rotation seen in the rake vectors. The significant rotation of the rake vectors along with the poor fit of the single source mechanism with long period Rayleigh Waves (left column of Fig. 3b) indicates a potentially complex event, which may require a multiple point source solution. The left column of Fig. 3b shows the predicted ultra-long period Rayleigh-wave motions, in red, for the single source solution, versus the observed W-phase waveforms in black. The single source solution shows discrepancies in both phase and amplitude. Such discrepancies, especially with regard to phase, suggest that the single source solution may not be fully describing the event.

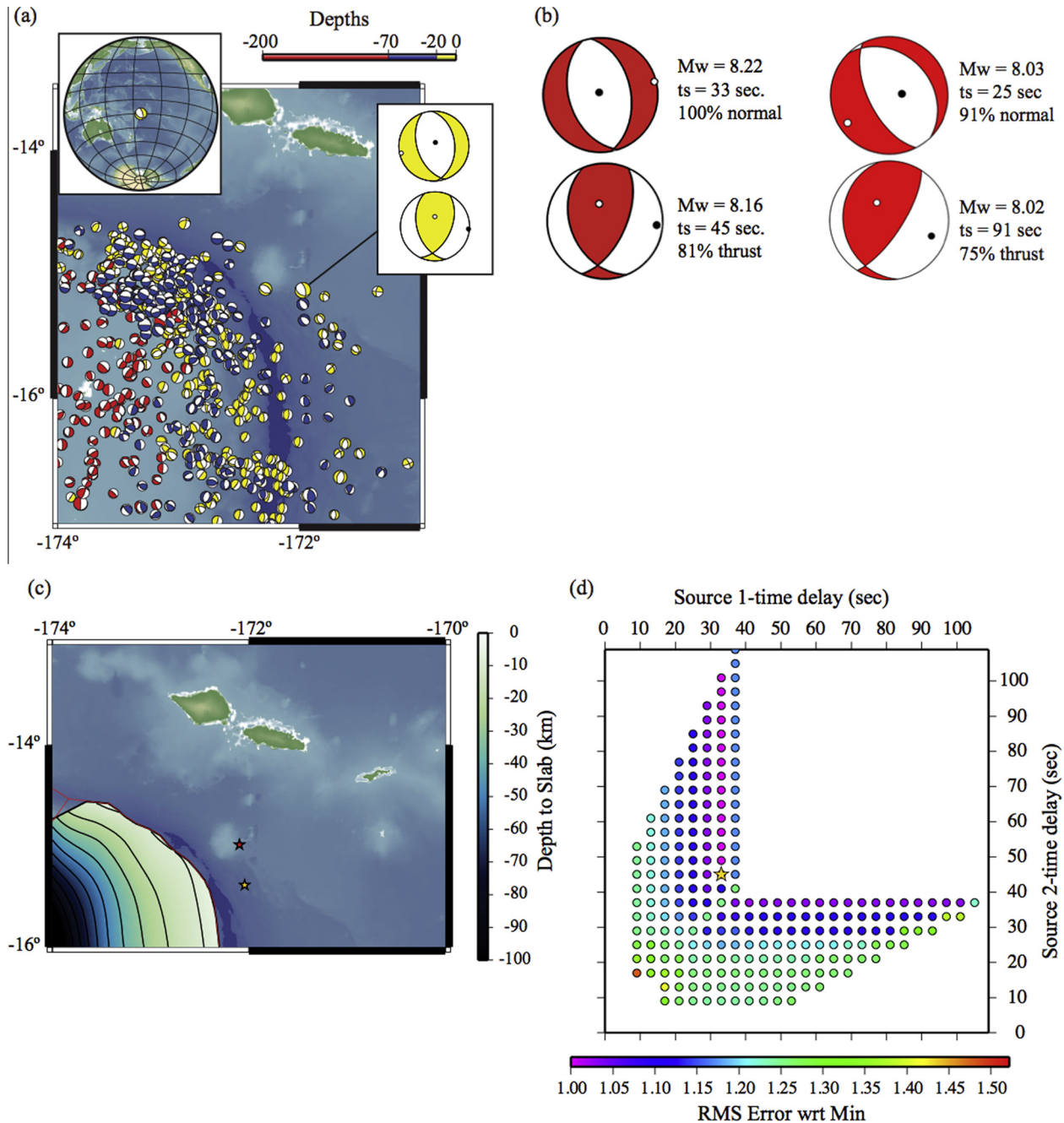
After performing the W-phase single source inversion, a two point source inversion is performed. Fig. 2b (left) shows the focal mechanisms derived for the two point source solution. For operational-based, real-time double point source W-phase inversions, the centroid location of both events is initially fixed at the centroid location of the single source event, to save computation time. We find that this constraint does not notably influence the results of the inversion while significantly decreasing the time taken to derive the final solutions. The result obtained from the time shift grid search performed during the double source inversion is shown in Fig. 2d, implying that the initial normal event occurred at a time delay of 33 s and was followed by a thrust event with a time delay of 45 s. The right column of Fig. 3b shows a comparison with the subsequent two point source solution at the same stations used for the single source solution. The phase and amplitude discrepancies have been corrected, implying that the two point source model provides the better solution. The AIC test performed for the single source and double source inversion also indicates that the double source model should be selected.

Fig. S2 shows the results of a double source W-phase inversion if a centroid grid search is also performed. In this case the focal mechanisms of the two solutions still show that there was a normal sub-event followed by a thrust sub-event, occurring at around the same times as in the fixed centroid solution; however now the second sub-event has been relocated to the northwest of the initial event. Fig. S2b shows the new centroid locations of the two events. Since the centroids were allowed to differ from the single source event location, grid searches were performed to find the optimal

**Table 2**

A sample of the results from running the technique introduced in this paper for all earthquakes since January 1, 2000 with magnitude 7.5 or greater. The columns contain the event name, date the event occurred, magnitude(s), whether a single source or double point source inversion was used, selected time delay(s) and the focal mechanism(s) obtained. Note that if a double point source model was selected, the magnitudes and focal mechanisms obtained using a fixed centroid location are shown in order of occurrence. Additionally, if the event was rerun with additional constraints, the solution found using the constrained run is shown. For the full list of results see Table S1 in the Supplementary figures.

Event	Date	M <sub>w</sub> (s)	Time Delay(s)	Half-Duration(s)	Focal Mechanism(s)
Kirakira, Solomon Islands	2014-04-12	7.72, 7.55	26 sec., 42 sec.	26 sec., 11.7319 sec.	
Panguna, Papua New Guinea	2014-04-19	7.51	12 sec.	12 sec.	
Scotia Sea	2013-11-17	7.81	43 sec.	43 sec.	
Awaran, Pakistan	2013-09-24	7.41, 7.63	9 sec., 29 sec.	9 sec., 24 sec.	
Haida Gwaii, Canada	2012-10-28	7.2, 7.75	13 sec., 37 sec.	13 sec., 31.4842 sec.	
Sumatra	2012-04-11	8.45, 8.37	38 sec., 70 sec.	38 sec., 63.6687 sec.	
Samoa Islands region	2009-09-29	8.03, 8.02	25 sec., 91 sec.	25 sec., 91 sec.	
Andaman Islands, India region	2009-08-10	7.25, 7.46	9 sec., 33 sec.	9 sec., 25.7540 sec.	
Sichuan, China	2008-05-12	7.78, 7.63	37 sec., 67 sec.	37 sec., 67 sec.	
Coast of central Peru	2007-08-15	8.09	62 sec.	62 sec.	
Kuril Islands	2007-01-13	8.27, 8.12	39 sec., 55 sec.	39 sec., 24.4148 sec.	
New Ireland region	2005-09-09	7.45, 7.49	19 sec., 35 sec.	19 sec., 28.7227 sec.	
West coast of northern Sumatra	2004-12-26	8.45, 9.14	27 sec., 131 sec.	27 sec., 123.6620 sec.	
Central Alaska	2002-11-03	7.63, 7.92	19 sec., 39 sec.	19 sec., 34 sec.	
North coast of Papua, Indonesia	2002-10-10	7.66, 7.43	26 sec., 38 sec.	26 sec., 15.3154 sec.	
Gujarat, India	2001-01-25	7.59, 7.4	12 sec., 32 sec.	12 sec., 16.4963 sec.	
Wharton Basin	2000-06-18	7.85	3 sec.	3 sec.	
Enggano	2000-06-04	7.99, 7.93	24 sec., 42 sec.	24 sec., 35.9166 sec.	



**Fig. 2.** (a) Historical seismicity for the area surrounding the 2009 Samoa great earthquake. The focal mechanisms show events of magnitude 5.0 and greater from January 1976 to November 2014 colored according to depth. The top right inset shows the corresponding W-phase two point source solution for the event. The global location of the event is shown in the top left inset. (b) The focal mechanisms obtained using the two point source W-phase inversion technique with fixed centroid location (left) for the September 29, 2009 Samoa event. The focal mechanisms obtained using the two point source W-phase inversion technique for the September 29, 2009 Samoa event using a centroid grid search with depths and time shifts fixed to correspond to Lay 2010 (right). (c) Location of the first (gold star) and second (red star) sub-events using a centroid grid search to determine optimum locations where depths and time shifts correspond to Lay 2010. The blue shading indicates depth to slab in km. (d) A sample of the point source time delays explored for the two sources. The color of each point corresponds to the RMS error with respect to the minimum error. A gold star marks the selected point source delay times at 115 s along the source 1 axis and 35 s along the source 2 axis. (For interpretation of the references to colour in this figure legend, the reader is referred to the web version of this article.)

depths, and horizontal locations. The results of the searches are shown in Figs. S2c and S2e.

Previously published literature has also found that the 2009 Samoa event was a multiple source event. A 2010 study by Bevan et al. found that the Samoa event was a double source event that consisted of a  $M_w$  7.9 normal sub-event followed by a  $M_w$  8.0 thrust sub-event to the southeast. Another study, a 2010 work by Lay et al., found that the 2009 Samoa event was actually three sub-events: a  $M_w$  8.1 normal sub-event followed by two  $M_w$  7.8 thrust

sub-events. The initial normal event was modeled to describe the first 60–100 s of the source process, while subsequent energy was attributed to the triggered thrust sub-events. Since we use a maximum of two events, the two thrust sub-events of the Lay et al. study were combined into our single thrust sub-event, as described in Figs. 4 and S2. This merging of the two  $M_w$  7.8 sub-events explains the larger magnitude ( $M_w$  8.04) of the thrust event found in our study. The time shifts found here for the two sub-events are also consistent with the time shifts found for the three

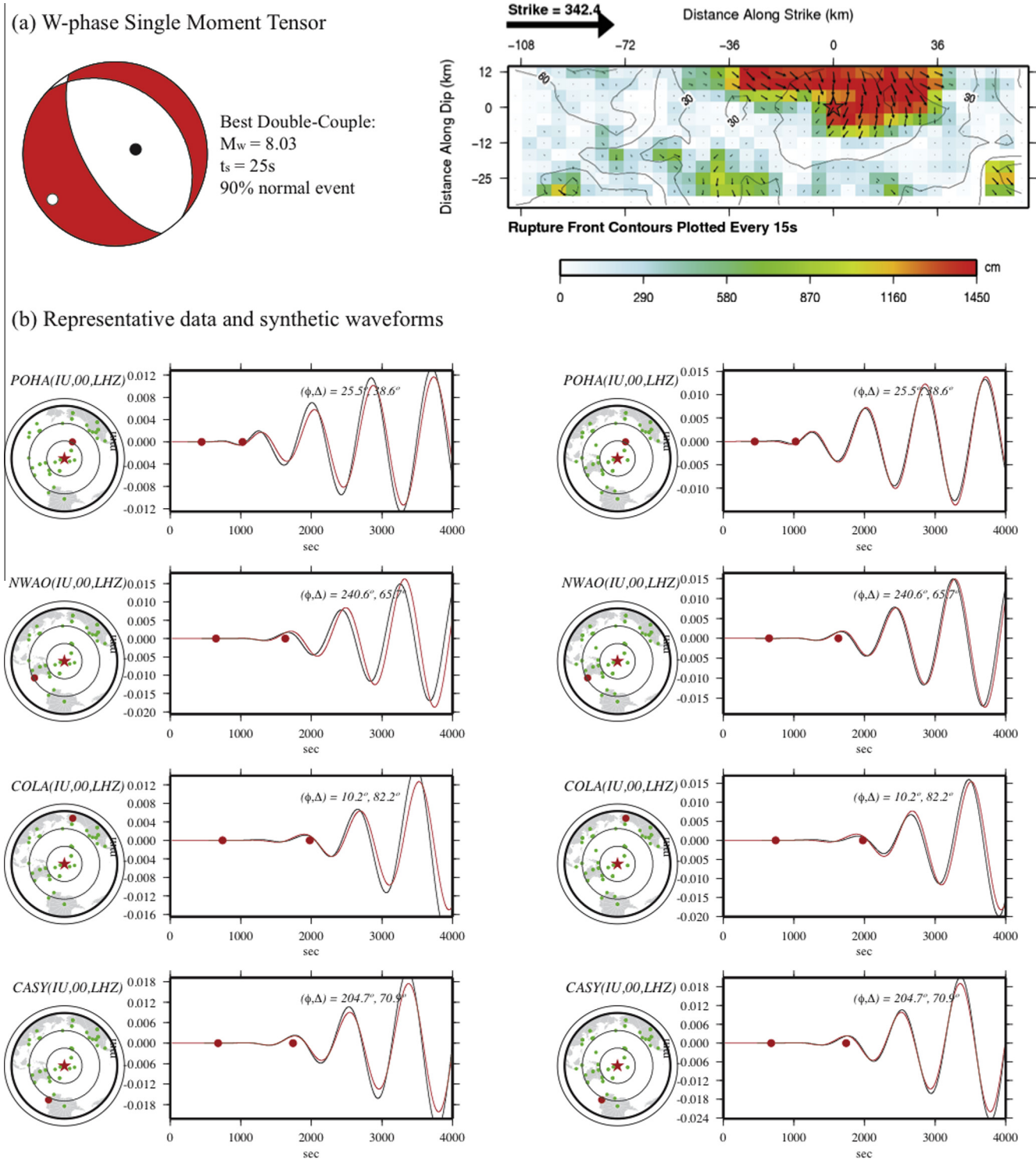


**Fig. 3.** (a) Single source moment tensor W-phase inversion solution shown alongside a cross section of the slip distribution for the September 29, 2009 Samoa event. (b) Surface wave motion for simple and composite models. Ultra-long period (774–1000 s) Rayleigh-wave motions (black) for the W-phase point source solution (red, on left) and for the W-phase double source solution (red on right). The W-phase interval is indicated by the red dots on the traces. See Fig. S1 in the supplementary figures for additional waveform comparisons. (For interpretation of the references to colour in this figure legend, the reader is referred to the web version of this article.)

sub-events by Lay et al., with our thrust sub-event corresponding to the later of the two thrust sub-events in the Lay et al. study. If we fix the depths of the two events at 18 km (as was done by Lay et al.) and set the time shifts to correspond to those selected by Lay et al. for the first two sub-events, we obtain the results shown in Fig. 2b (right) and Fig. 2c. These adjustments result in a

$M_w$  8.03 normal sub-event followed by a  $M_w$  8.02 thrust sub-event occurring to the southeast of the original sub-event. The second event is not well constrained which results in the preferred location of the second event being outside of the Tonga subduction zone. The location of the second event can be constrained so that only locations within the subduction zone are considered; the

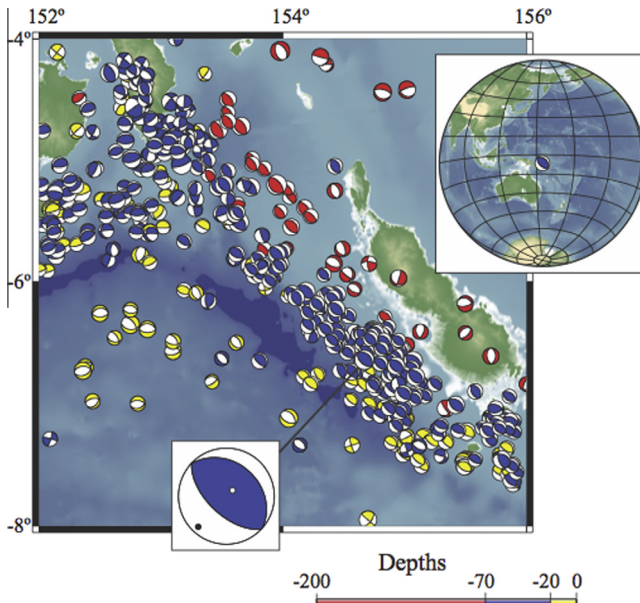


**Fig. 4.** Historical seismicity for the area surrounding the 2014 Panguna earthquake. The focal mechanisms show events of magnitude 5.5 and greater from January 1976 to November 2014 colored according to depth. The bottom left inset shows the corresponding W-phase point source solution for the event. The global location of the event is shown in the top right inset.

results from including this additional constraint are shown in Fig. S3. These results are in agreement with those found by Lay et al. (2010b).

Constraining components of the inversion to fit the finite fault model, seismic wave data, or the tectonic setting of the event, as was done here for the 2009 Samoa great earthquake, can also be attempted in real-time to obtain more accurate results, if preliminary results from unconstrained searches seem questionable. Another example of this approach can be seen in Fig. S4, which describes results from performing a double point source inversion for the 2008 Sichuan earthquake. The finite fault model of the Sichuan event suggests that a thrust event near the hypocenter was followed by a strike-slip sub-event to the northeast. In order to remain consistent with the finite fault model, we constrain the dip of the first sub-event to 33° and the dip of the second sub-event to 60° prior to the inversion as well as constraining the times to match Nakamura et al. (2010). Constraining the inversion in this manner resulted in a  $M_w$  7.81 thrust sub-event followed by a  $M_w$  7.63 strike-slip sub-event to the northeast, consistent with other studies (Nakamura et al., 2010).

The depths, time shifts, and focal mechanisms selected when using a time shift grid search followed by a centroid grid search, regardless of whether stations are removed, are very similar to those selected when performing only a time shift grid search, but result in a much slower run time. Since the solutions derived using only a time shift grid search are acceptable, it is preferable to use this inversion technique during real-time operations, reserving the centroid grid search inversion for research purposes only.

### 3.2. Single source model – 2014 Panguna earthquake

The 2014 Panguna earthquake was selected to represent a full run for a single source event. The Panguna earthquake was a magnitude 7.51 event that occurred near Papua New Guinea, on April 19. The single source solution selected using our two-stage inversion technique is shown in the inset of Fig. 4. The CMT was found to be a thrust event (Fig. 5a) and is consistent with other historical earthquakes in the area. A time shift of 12 s was selected using

the grid search, agreeing with the moment rate function derived for the event ([http://earthquake.usgs.gov/earthquakes/eventpage/usb00pr89#scientific\\_finitefault](http://earthquake.usgs.gov/earthquakes/eventpage/usb00pr89#scientific_finitefault), 2014). Additionally, the cross section of the slip distribution shown in Fig. 5a shows consistent slip throughout the rupture, suggesting a single source estimate can fully describe the event. Fig. 5b compares the data and synthetic waveforms using a passband of 0.002–0.0067 Hz, showing good agreement between the two. In order to ensure that a double source model would not provide any improvements upon the single source solution, the ultra-long period Rayleigh-wave motions were compared to predictions for the W-phase point source solution and for the W-phase two point source solution. Unlike the results of this comparison for the Samoa earthquake (Fig. 3b) using a two point source solution did not improve waveform fits for the Panguna event (Fig. 5c). In addition to the lack of visible improvement in waveforms when extending from a single to a double source, the AIC test also indicates that a single source model is most appropriate for this event. Since no improvement was made to the predictions for the W-phase solution when a two point source case was considered, the AIC test recommends a single source model, and since the single source solution has excellent agreement with the moment rate function, representative data, and historical seismicity, we conclude that a single source model provides a better representation for this earthquake.

### 3.3. Discussion

In this section, we will compare our results with solutions derived by other authors (e.g., Duputel et al., 2012b). Solutions for events that occurred after 2010 that were not modeled by Duputel et al. (2012) are compared to information in ComCat. When discussing the strike, dip, and rake of the events standard notation is used, where  $\phi$  is strike,  $\delta$  is dip, and  $\lambda$  is rake.

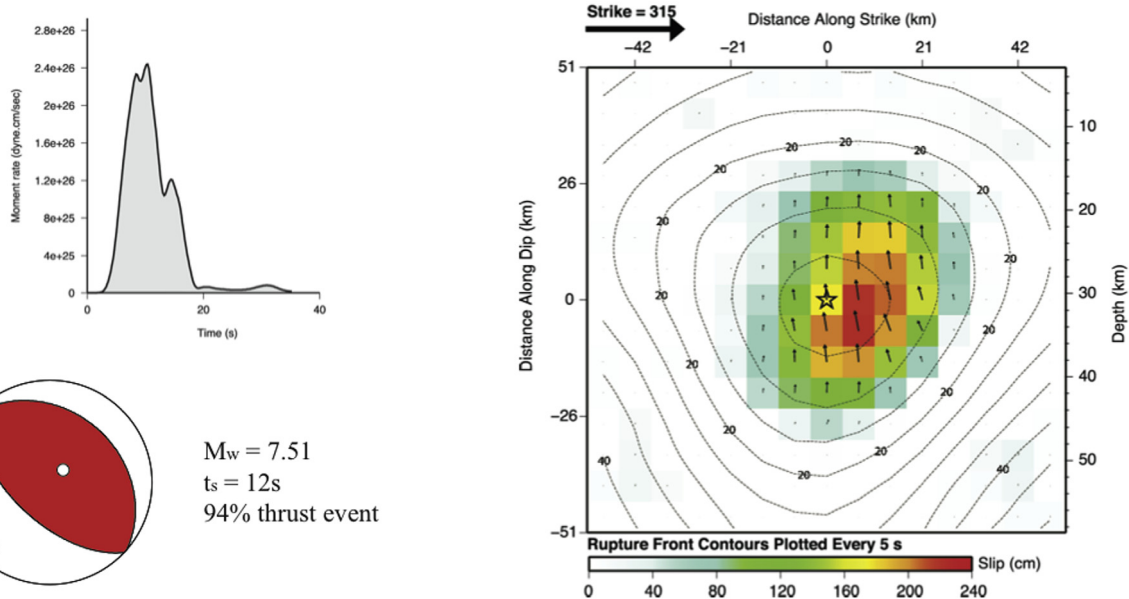
#### 3.3.1. Single source events

To quantitatively compare our single source solutions with gCMT solutions, the angular parameter  $\Phi$  ( $M_{wcmt}, M_{gcmt}$ ) was found and our magnitudes were compared against the gCMT magnitudes. The angular parameter  $\Phi$  for each event is defined as the smallest rotation linking the two sets of  $M_{wcmt}$  and  $M_{gcmt}$  principal axes (Duputel et al., 2012). The difference in magnitude for each event is shown in Fig. 6(a); Fig. 6(b) gives the results from comparing the magnitudes found here with the corresponding gCMT magnitudes. Overall, 91% of the magnitudes found here for single source events were within a 0.1 magnitude unit difference of the gCMT magnitude and 99% were within a 0.2 magnitude unit difference. Our magnitudes were also compared to the magnitudes found by Duputel et al. (2012b) using WCMT solutions. When comparing to the Duputel magnitudes, 97% of our single source events were within a 0.1 magnitude unit difference and 100% were within a 0.2 magnitude unit difference.

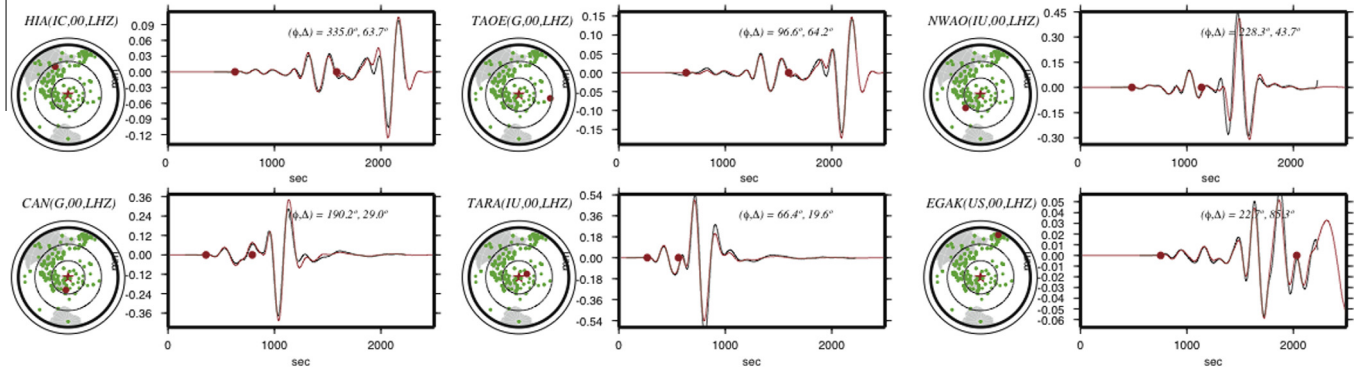
Fig. 7 shows the angular parameter found for each event. We selected  $\Phi < 35^\circ$  (shown by the red dashed line in Fig. 7) to be an acceptable value for the angular parameter classifying events within this range as being in good agreement with the gCMT solution. Overall 96% of the single source events considered had  $\Phi < 35^\circ$ , with only three events having a larger angular parameter.

In order to determine how well classified our events were, the Akaike weights for the events were calculated and used to find the probability that the selected model was the better representation for the event being considered (Fig. 8). All events with a model probability greater than 90% are considered well classified. If the model probability for the event is found to be less than the selected cutoff, the event should be evaluated further to determine if there is any complexity present in the event that would be better repre-

## (a) Model for single-source event



## (b) Representative data and synthetic waveforms



## (c) Ultra-long period waveform comparisons

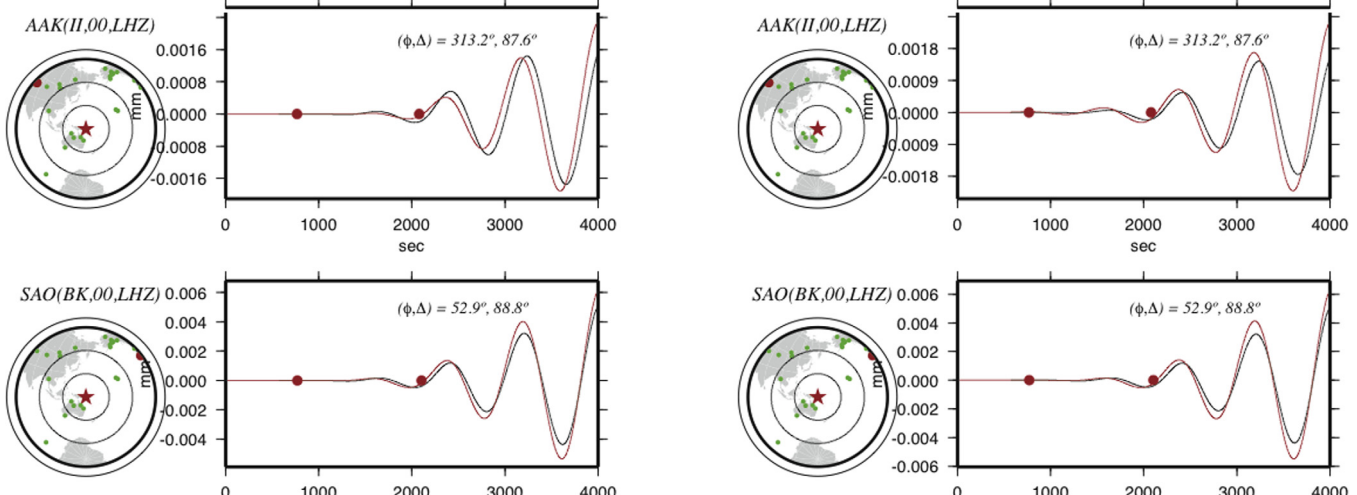


**Fig. 5.** (a) Moment rate function and double-couple focal mechanism shown alongside a cross section of slip distribution for the April 19, 2014 Panguna event. (b) Representative data (black) and synthetic (red) waveforms using a passband of 0.002–0.0067 Hz. The red dots indicate the W-phase interval. (c) Ultra-long period (774–1000 s) Rayleigh-wave motions (black) compared to predictions for the W-phase point source solution (red, on left) and for the W-phase double source solution (red, on right) for the 2014 Panguna earthquake. In both figures the W-phase interval is indicated by the red dots on the traces. (For interpretation of the references to colour in this figure legend, the reader is referred to the web version of this article.)

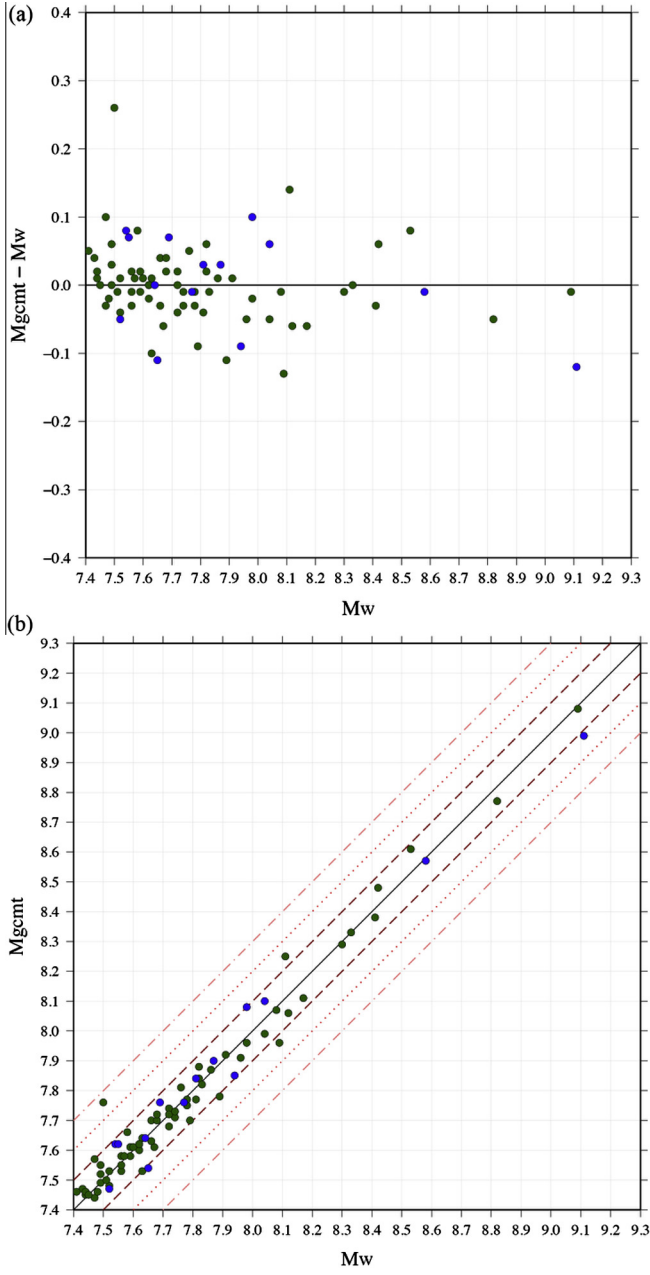


**Fig. 6.** The difference between the magnitudes found for our single source solutions (green circles) and the corresponding gCMT magnitudes (top). The comparison between our single source magnitudes and those found using gCMT (bottom). For this comparison, double source events were combined into single centroid solutions, indicated by blue circles. (For interpretation of the references to colour in this figure legend, the reader is referred to the web version of this article.)

sented by a multiple source. Three of our single source events (2003 Carlsberg, 2007 Fiji, 2012 Costa Rica) were found to be below the prescribed cutoff with probabilities of 89%, 59%, and 52%, respectively. In all three of these cases, analysis of the finite fault models and the moment rate functions for the events indicated little to no complexity, which is in agreement with the single source classification.

The 2013 Scotia Sea, 2013 Sea of Okhotsk, 2007 Peru and the 2000 Wharton basin earthquakes were found to be single source events using the techniques presented here; however, they were found to be multiple source events by other authors. For the 2013 Scotia Sea earthquake, Ye et al. (2014) found that a solution made up of three strike-slip sub-events best represented the event.

The Ye et al. solution was comprised of three contiguous fault segments where the second segment ruptured from ~70 to 100 s and the third segment ruptured from ~110 to 120 s. Performing a double source inversion for this event, we obtain a  $M_w$  7.56 strike-slip sub-event with a time delay and half-duration of 21 s followed 16 s later by a  $M_w$  7.92 strike-slip sub-event with a half-duration of 32 s. Both of our sub-events fall within the initial moment release seen on the moment rate function and the duration of the sub-events ends prior to the rupture of the second segment found by Ye et al. (2014). Vallée and Satriano (2014) also studied the 2013 Scotia Sea earthquake, examining the rupture expansion of the event. Although they did not model this as a multiple source event, instead using the GCMT single source representation, the study found that the event exhibited two main episodes of seismic slip both temporally and spatially and described the event as occurring in a structurally complex area. Performing a single source inversion results in a  $M_w$  7.92 strike-slip event with a time delay and half-duration of 43 s. For this event, the double source solution does not improve upon the single source solution so the single source solution was selected as the better model.

For the 2013 Sea of Okhotsk earthquake, we found the best representation of the event using a fixed centroid location to be a  $M_w$  8.19 normal faulting sub-event. This event was previously found to be a multiple source event by Chen et al. (2014), who modeled the event as six sub-events occurring very close together in time and ranging in magnitude from 6.91 to 7.88. Zhan et al. (2014) also found this event to be a multiple source event. The model selected by Zhan et al. (2014) was made up of four sub-events where the initial sub-event occurred at ~8 s with the rupture ending at about 30 s. It should be noted that in the case of Chen et al. (2014), the solution of six sub-events was presubscribed, not selected as the best model. If we perform a full centroid grid search for this event, a  $M_w$  8.36 normal faulting sub-event ( $\phi = 14.5$ ,  $\delta = 80.2$ ,  $\lambda = -87.4$ ) with a time delay and half-duration of 23 s followed by a  $M_w$  7.83 thrust faulting sub-event ( $\phi = 127.1$ ,  $\delta = 23.9$ ,  $\lambda = 8.6$ ) with a time delay of 59 s and a half-duration of 50.9631 s is obtained. The time delays selected for the double source solution are in disagreement with those found by Zhan et al. (2014) and Chen et al. (2014) and the second sub-event is not in agreement with the finite fault model for this event which indicates predominately normal faulting motion. The lack of agreement of the second sub-event and time delays combined with the results of the AIC test indicates that the single source solution is a better representation for this event.

The August 15, 2007 Peru earthquake was found here to be a single source event when using a fixed centroid location. Lay et al. (2010a) previously found this to be a double source solution consisting of two thrust sub-events, a  $M_w$  7.8 ( $\phi = 324$ ,  $\delta = 22$ ,  $\lambda = 78$ ) followed by a  $M_w$  8.0 ( $\phi = 324$ ,  $\delta = 22$ ,  $0.35em\lambda = 73$ ). When modeling this solution, Lay et al. (2010a) separated the two sub-events by 60 s in time and had the hypocenters separated by 45 km along strike and 30 km along dip. If we also perform a full centroid grid search inversion assuming the same timings as Lay et al. (2010a), we obtain a  $M_w$  7.61 thrust faulting sub-event ( $\phi = 327.9$ ,  $\delta = 35.6$ ,  $\lambda = 73.6$ ) followed by a  $M_w$  8.20 thrust faulting sub-event ( $\phi = 321.4$ ,  $\delta = 11.9$ ,  $\lambda = 58.1$ ). In this case, if the timings are constrained to match those selected by Lay et al. (2010a), a double source solution is found to be a better representation of this event.

The June 2000 Wharton Basin earthquake was also previously found to be composed of multiple sub-events (Robinson et al., 2001; Abercrombie et al., 2003). Robinson et al. (2001) found the Wharton Basin earthquake to be made up of two strike-slip sub-events occurring 15 s apart with a total magnitude of  $M_w$  7.8. Abercrombie et al. (2003) combined broadband body wave modeling and aftershock relocations to study the rupture geometry for

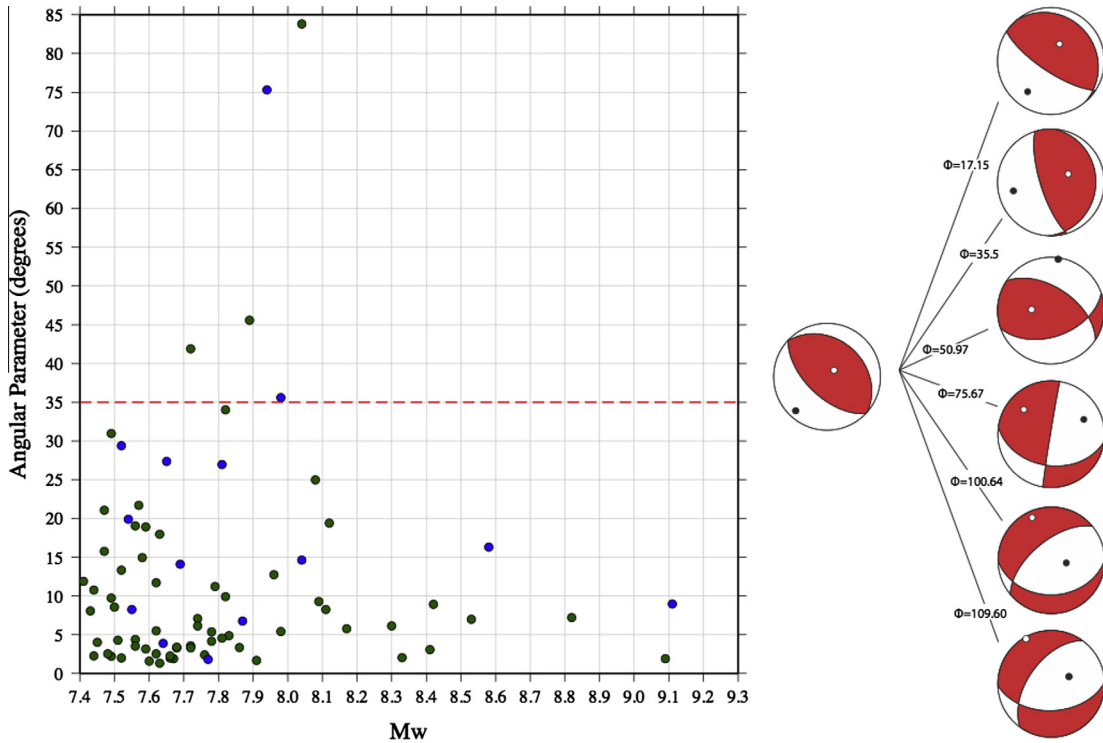


**Fig. 7.** The angular parameter  $\Phi$  ( $M_{\text{wcmt}}, M_{\text{gcmt}}$ ) found for all  $M_{\text{w}} \geq 7.5$  + earthquakes that have occurred since January 1, 2000. The red dashed line indicates  $\Phi = 35^\circ$ , the cutoff used to determine if the WCMT event and the gCMT event are in good agreement in terms of the moment tensor. Green circles indicate single source solutions and blue circles denote double source events were combined into single centroid solutions. To the right of the graph is a selection of focal mechanisms comparisons. The focal mechanism pairs connected by a line were compared; the angular parameter found for each pair is indicated. (For interpretation of the references to colour in this figure legend, the reader is referred to the web version of this article.)

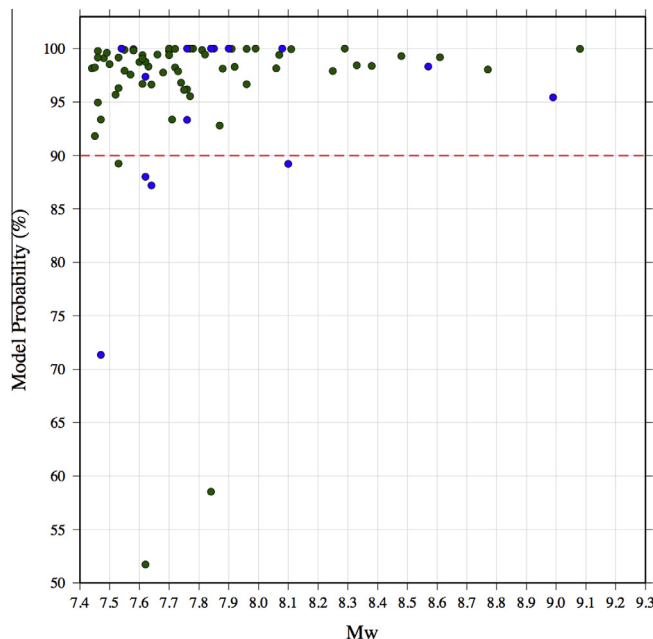


**Fig. 8.** The probability that the selected model (given as a percentage) is the better representation of the event under consideration shown for events classified as single source models (green circles) and double source models (blue circles). The red dotted line indicates a 90% probability that the model is better; this value is used as a cutoff to determine if an event is of questionable classification. (For interpretation of the references to colour in this figure legend, the reader is referred to the web version of this article.)

the event, finding that a  $M_{\text{w}} 7.76$  strike-slip sub-event followed by a  $M_{\text{w}} 7.44$  thrust sub-event was the better solution. Both authors point out that difficulties arise since the two events occur so close

together in time; Robinson et al. (2001) mention that the moment rate function for this event does not reflect the complexity of the rupture process and Abercrombie et al. (2003) use the fact that the two events occurred almost simultaneously to explain why their second event is poorly constrained.

Since the two sub-events are expected to occur so close together in time, the long-period nature of our inversion process may increase the difficulty when attempting to resolve the two mechanisms, which could then lead to a less accurate double source representation. If we model the Wharton Basin earthquake as a double source event, we obtain a strike-slip sub-event ( $M_{\text{w}} 7.89$ ) with a time delay of nine seconds followed 28 s later by a smaller strike-slip sub-event ( $M_{\text{w}} 7.54$ ). The magnitudes, time delay separation, and first sub-event are in agreement with the solutions found by both Robinson et al. (2001) and Abercrombie et al. (2003); however, the mechanism of our second sub-event was found to be a strike-slip rather than a reverse slip. The lack of agreement of the second sub-event combined with the results of the AIC test indicates that the  $M_{\text{w}} 7.85$  single source strike-slip event was a better representation for this earthquake.

### 3.3.2. Double source events

All events classified as double source events were compared to solutions found by other authors (Fig. 9). If an event had not been previously modeled as a double source event, we ensure that our results are consistent with the tectonics of the area; the solutions obtained for these events are shown in Table 2 (using a fixed centroid location) and Table S1 (using a centroid location grid search). It should be noted that when an event is selected as a double source it does not mean that the best representation of the event is two sources; rather the selection indicates that the event is better represented as a complex event. A more in depth discussion of

all double source events is given in the [Supplementary material](#) ([USGS, 2000, 2005, 2012, 2014b; Aagaard et al., 2004; Ji et al., 2004; Oglesby et al., 2004; Meng et al., 2012; Lay et al., 2013a; Cassidy et al., 2014](#)).

[Fig. 9](#) shows how our solutions compared to previous studies. The first column depicts the focal mechanisms, magnitudes, time delays, half-durations, strike, dip, and rake of our solutions. In the second column, the corresponding information obtained by previous authors is shown alongside the reference from which the focal mechanisms and data were obtained. The third column is used only when we applied constraints during our run in order to match the solutions found by other authors and shows the constrained solution as well as lists the applied constraints. Of the 14 events classified as double sources, 3 events (2007 Kuril, 2004 Sumatra, 2001 Gujarat) appeared to have major discrepancies with either the solutions found by other authors or with the moment rate function and finite fault analysis for the corresponding single source solution.

For the January 13, 2007 Kuril earthquake, our solution of a normal faulting sub-event followed by a thrust faulting sub-event is not in agreement with the finite fault analysis of the single source solution, which does not indicate any thrust faulting. This event has previously only been modeled as a single source event ([Ammon et al., 2008; Fujii and Satake, 2008; Lay et al., 2009](#)), however, the moment rate function indicates potential complexity in the solution that may be better represented by a multiple source event.

The December 26, 2004 Sumatra earthquake was previously found to be a complex event by multiple authors including [Tsai et al. \(2005\)](#) who used a multiple CMT analysis to determine that the best representation was a five sub-event solution comprising five thrust sub-events ranging in magnitude from  $M_w$  8.54 to  $M_w$  9.31 ([Ammon et al., 2005; Stein and Okal, 2005; Banerjee et al., 2005; Park et al., 2005](#)). Using a fixed centroid location, we obtained a  $M_w$  8.45 normal faulting sub-event ( $\phi = 334.9$ ,  $\delta = 6.9$ ,  $\lambda = -111.7$ ) with time delay and half-duration of 27 s followed by a  $M_w$  9.14 thrust faulting sub-event ( $\phi = 332.1$ ,  $\delta = 5.6$ ,  $\lambda = 107.5$ ) with a time-delay of 131 s and a half-duration of 123.6620 s. Performing a full centroid grid search results in a  $M_w$  8.14 normal faulting sub-event ( $\phi = 344.7$ ,  $\delta = 19.6$ ,  $\lambda = -96.3$ ) followed by a  $M_w$  9.11 thrust faulting sub-event ( $\phi = 327.1$ ,  $\delta = 6.2$ ,  $\lambda = 100.6$ ). In both cases the normal faulting nature of the first sub-event is in disagreement with the thrust faulting solutions found by [Tsai et al. \(2005\)](#). For this event, the source time function used by [Tsai et al. \(2005\)](#) indicates that this event lasted around 600 s with the centroid time delay of the first sub-event occurring between 50 and 100 s and the time delay of the second sub-event occurring between 150 and 200 s. This indicates that the time delays found for our two sub-events are both occurring too soon. Due to the restrictions placed on the time delays and half-durations during the time shift grid search, our second sub-event does not ever test time delays that correspond to the 150–200 s delay selected by [Tsai et al. \(2005\)](#). If the time delay and half-duration for the first sub-event are fixed at 100 s and the time delay and half-duration for the second sub-event are fixed at 200 s, we obtain a  $M_w$  9.0 thrust sub-event ( $\phi = 301.6$ ,  $\delta = 3.8$ ,  $\lambda = 81.2$ ) followed by a  $M_w$  9.12 thrust sub-event ( $\phi = 345.0$ ,  $\delta = 8.6$ ,  $\lambda = 106.6$ ). The agreement between the constrained solution, the solutions found by [Tsai et al. \(2005\)](#) and the finite fault model indicates that a longer time delay than is allowed by our technique is required in order to obtain an accurate solution for this event.

The January 25, 2001 Gujarat earthquake has not been studied in depth previously, however, the moment rate function and finite fault analysis for the single source solution both indicate potential complexity ([http://earthquake.usgs.gov/earthquakes/eventpage/usps000a8ds#scientific\\_finitefault, 2001](#)). Using a fixed centroid

location, we obtained a  $M_w$  7.59 thrust faulting sub-event ( $\phi = 63.6$ ,  $\delta = 60.2$ ,  $\lambda = 55.9$ ) with a time delay and half-duration of 12 s followed by a  $M_w$  7.4 normal faulting sub-event ( $\phi = 56.8$ ,  $\delta = 85.0$ ,  $\lambda = -89.2$ ) with a time delay of 32 s and a half-duration of 16.4963 s. Performing a centroid grid search results in a  $M_w$  7.58 thrust faulting sub-event ( $\phi = 118.9$ ,  $\delta = 61.2$ ,  $\lambda = 123.9$ ) followed by a  $M_w$  7.14 normal faulting sub-event ( $\phi = 122.4$ ,  $\delta = 75.4$ ,  $\lambda = -91.9$ ). In both cases, although the time delays match the moment rate function, the normal faulting sub-event is not in agreement with the finite fault model, which does not indicate any normal faulting. The lack of agreement between the second sub-event and the finite fault model may indicate that using two sub-events is not the best representation of this event.

Overall, the double source W-phase inversion technique using only a time shift grid search is able to derive magnitudes and time shifts for sub-events that are consistent with the moment release for the event and the tectonics of the area. When the double source solutions are combined into a single event, 100% are within 0.2 magnitude units of the corresponding gCMT magnitudes and 79% are within 0.1 magnitude units of the magnitudes found by [Duputel et al. \(2012b\)](#). Discrepancies in magnitude or timing can often be corrected simply by performing a full centroid grid search. Events can be constrained prior to inversion to account for the tectonics of the area, if additional and independent information is available to guide such a choice, which can result in more accurate solutions. This was demonstrated in the cases of the 2009 Sumatra earthquake and the 2008 Sichuan earthquake. The angular parameters derived when the double source events were combined into single centroid solutions also show that the majority of our events are in good agreement with gCMT solutions, with 86% of all combined events having  $\Phi < 35^\circ$ .

As with the single source events, in order to determine how well classified our events were, the Akaike weights for the events were calculated ([Fig. 8](#)). There were four double source events (2001 Gujarat, 2005 New Ireland, 2007 Kuril, 2009 Andaman) with model probability below 90 percent (88%, 87%, 89%, 71%, respectively). Both the 2001 Gujarat and the 2007 Kuril earthquake were singled out prior to the evaluation of the likelihood of the model due to discrepancies found when the solutions were compared to their respective moment rate function and finite fault analysis for the corresponding single source solution. In the case of the New Ireland earthquake, the solution obtained using a fixed centroid grid search was in agreement with the moment rate function and finite fault model; however, performing an inversion incorporating a centroid grid search determined that a single source solution is a better representation. The 2009 Andaman earthquake was not singled out prior to evaluating the events using their Akaike weights since it is in agreement with the moment rate function and finite fault analysis for the single source solution ([http://earthquake.usgs.gov/earthquakes/eventpage/usps000h05x#scientific\\_finitefault, 2009](#)).

The waveforms for each of the four selected events were examined and the events were rerun with poor fits removed. The solutions obtained from the reruns of all four events indicated that a single source solution was a better representation once poor waveform fits were eliminated. In order to ensure that removing poorly fitting waveforms would not result in a single source classification for all events classified as double sources, the 2012 Sumatra earthquake, which had a 98% probability of being a double source solution, was also rerun with poorly fitting waveforms removed. The rerun for the 2012 Sumatra event indicated that even with the poor fits removed, this event should still be classified as a double source event. The reclassification of the four events indicates that for events considered questionably classified, the quality of the waveform fits is an important variable and any events selected as questionable classifications should be reevaluated with

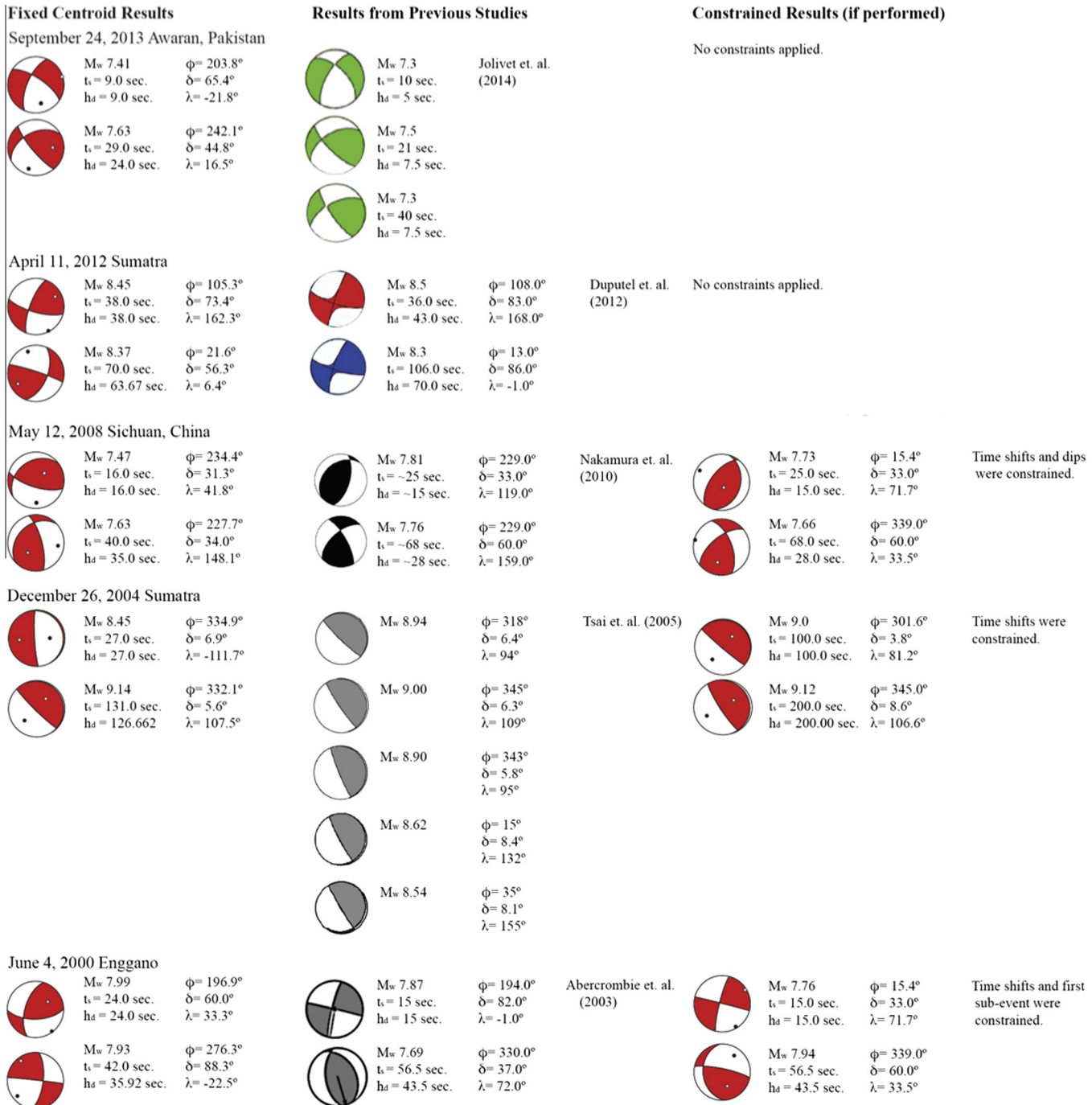


**Fig. 9.** Comparisons of the results obtained using the technique presented here with a fixed centroid location and results obtained in previous studies. For each sub-event the magnitude, time delay, half-duration, strike, dip, and rake are given (when available). If a constrained run was performed, the new solution is shown alongside the constraints that were applied.

poor waveform fits removed in order to determine the best classification.

The results obtained for the 2004 Sumatra event indicated that in a real time run events with long durations can be correctly classified as multiple source events, however, may not be able to obtain accurate solutions due to the restrictions imposed during the time shift grid search. Although these events may not be singled out as questionable classifications, the half-duration found for the single source solution would indicate that the event being considered has a long duration and therefore may have problems obtaining accurate focal mechanisms during the double source

inversion. The 2004 Sumatra earthquake, for example, had a half-duration of 140 s for its single source solution. This half-duration was much longer than the half-durations found for the other events considered here, with the 2006 Java event having the next largest half-duration at 72 s. If a single source solution is found to have a long duration, the restrictions placed on the half-duration and time delay within the double source inversion could be altered to account for the longer duration of the event or additional constraints could be placed on the event in order to conform to the moment rate function and finite fault analysis of the single source solution.

## 4. Conclusions

The double source W-phase inversion has proven to be an accurate way to characterize complex earthquakes. Results can be obtained in real-time, with an average run time of 22.96 min on a quad-core CPU system with Intel Xeon E5620 processors running at 2.4 GHz, by performing a time delay grid search with fixed centroid locations within the inversion. Including a centroid grid search allows for more in-depth evaluations after an initial estimate of the double source has been derived. The ability to use either a time shift grid search or a full centroid grid search makes this technique useful for both real-time and research-based scenarios. Additionally, using an AIC test has proven to be a reliable technique for selecting the optimal model from either the single source or double source cases.

We have shown that the double source W-phase inversion technique used in conjunction with an AIC test can be successfully applied to very large earthquakes ( $M_w \geq 7.5$ ). In the future this technique could be extended to characterize N-source events in a similar manner, using an AIC test to determine the optimal number of sources that should be used to model the event. Additionally, further study could be applied to the use of the AIC test to determine if there are specific cases where other statistical tests could be used in conjunction with the AIC test or be supplemented for the AIC test to obtain more accurate results. The solutions obtained using the full centroid grid search version of this technique could also be used in the future to help characterize multiple planes for finite fault models.

## Acknowledgements

Figures in this manuscript were produced using the Generic Mapping Tools software package (Wessel and Smith, 1991). Gebco2014 bathymetry is used for all basemaps (Gebco\_2014 grid, 2014). Any use of trade, product, or firm names is for descriptive purposes only and does not imply endorsement by the U.S. Government.

## Appendix A. Supplementary data

Supplementary data associated with this article can be found, in the online version, at <http://dx.doi.org/10.1016/j.pepi.2015.09.005>.

## References

- Aagaard, B.T., Anderson, G., Hudnut, K.W., 2004. Dynamic rupture modeling of the transition from thrust to strike-slip motion in the 2002 Denali fault earthquake, Alaska. *Bull. Seismol. Soc. Am.* 94 (6B), S190–S201. <http://dx.doi.org/10.1785/0120040614>.
- Abercrombie, R.E., Antolik, M., Ekström, G., 2003. The June 2000 Mw 7.9 earthquakes south of Sumatra: deformation in the India-Australia plate. *J. Geophys. Res.: Solid Earth* 108 (B1), ESE-6, 1978, doi: 10.1029/2001JB000674, -1202.
- Akaike, H., 1972. Information theory and an extension of the maximum likelihood principle. In: Proc. 2nd Int. Symp. Information Theory, Supp. To Problems of Control and Information Theory, pp. 267–282. doi: 10.1007/978-1-4612-1694-0\_15.
- Akaike, H., 1974. A new look at the statistical model identification. *IEEE Trans. Autom. Control* 19 (6), 716–723. [http://dx.doi.org/10.1007/978-1-4612-1694-0\\_16](http://dx.doi.org/10.1007/978-1-4612-1694-0_16).
- Ammon, C.J., Ji, C., Thio, H.K., Robinson, D., Ni, S., Hjorleifsdottir, V., Wald, D., 2005. Rupture process of the 2004 Sumatra-Andaman earthquake. *Science* 308 (5725), 1133–1139. <http://dx.doi.org/10.1126/science.1112260>.
- Ammon, C.J., Kanamori, H., Lay, T., 2008. A great earthquake doublet and seismic stress transfer cycle in the central Kuril islands. *Nature* 451 (7178), 561–565. <http://dx.doi.org/10.1038/nature06521>.
- Banerjee, P., Pollitz, F.F., Bürgmann, R., 2005. The size and duration of the Sumatra-Andaman earthquake from far-field static offsets. *Science* 308 (5729), 1769–1772. <http://dx.doi.org/10.1126/science.1113746>.
- Beavan, J., Wang, X., Holden, C., Wilson, K., Power, W., Prasetya, G., Kautoke, R., 2010. Near-simultaneous great earthquakes at Tongan megathrust and outer rise in September 2009. *Nature* 466 (7309), 959–963. <http://dx.doi.org/10.1038/nature09292>.
- Burnham, K., Anderson, D., 1998. *Model Selection and Inference. A Practical Information Theoretic Approach*, second ed. Springer, New York.
- Canham, C. (Director), 2013, April 23. Model selection and multimodel inference. Likelihood methods and models in ecology. Lecture conducted from Cary Institute of Ecosystem Studies, Millbrook.
- Cassidy, J.F., Rogers, G.C., Hyndman, R.D., 2014. An overview of the 28 October 2012 M<sub>w</sub> 7.0 earthquake in Haida Gwaii, Canada: a tsunamigenic thrust event along a predominantly strike-slip margin. *Pure Appl. Geophys.* 171 (12), 3457–3465. <http://dx.doi.org/10.1007/s00024-014-0775-1>.
- Chen, Y., Wen, L., Ji, C., 2014. A cascading failure during the 24 May 2013 great Okhotsk deep earthquake. *J. Geophys. Res. Solid Earth* 119 (4), 3035–3049. <http://dx.doi.org/10.1002/2013JB010926>.
- Duputel, Z., Rivera, L., Kanamori, H., Hayes, G.P., Hirshorn, B., Weinstein, S., 2011. Real-time W phase inversion during the 2011 off the Pacific coast of Tohoku Earthquake. *Earth Planets Space* 3, 535–539. <http://dx.doi.org/10.5047/eps.2011.05.032>.
- Duputel, Z., Kanamori, H., Tsai, V.C., Rivera, L., Meng, L., Ampuero, J.P., Stock, J.M., 2012a. The Sumatra great earthquake sequence. *Earth Planet. Sci. Lett.* 351, 247–257. <http://dx.doi.org/10.1016/j.epsl.2012.07.017>.
- Duputel, Z., Rivera, L., Kanamori, H., Hayes, G., 2012b. W phase source inversion for moderate to large earthquakes (1990–2010). *Geophys. J. Int.* 189, 1125–1147. <http://dx.doi.org/10.1111/j.1365-246X.2012.05419.x>.
- Duputel, Z., Tsai, V.C., Rivera, L., Kanamori, H., 2013. Using centroid time-delays to characterize source durations and identify earthquakes with unique characteristics. *Earth Planet. Sci. Lett.* 374, 013, 92–100, <http://dx.doi.org/10.1016/j.epsl.2013.05.024>.
- Dziewonski, A.M., Chou, T.-A., Woodhouse, J.H., 1981. Determination of earthquake source parameters from waveform data for studies of global and regional seismicity. *J. Geophys. Res.* 6, 2825–2852. <http://dx.doi.org/10.1029/JB086iB04p02825>.
- Ekström, G., Nettles, M., Dziewonski, A.M., 2012. The global CMT project 2004–2010: centroid-moment tensors for 13,017 earthquakes. *Phys. Earth Planet. Inter.* 200, 1–9. <http://dx.doi.org/10.1016/j.pepi.2012.04.002>.
- Fujii, Y., Satake, K., 2008. Tsunami sources of the November 2006 and January 2007 great Kuril earthquakes. *Bull. Seismol. Soc. Am.* 98 (3), 1559–1571. <http://dx.doi.org/10.1785/0120070221>.
- Gahalaut, V.K., 2012. Great earthquakes as “surprises” or our lack of understanding. *Curr. Sci.* 102 (11), 1508.
- GEBCO\_2014 grid, 2014. Version 20141103. Retrieved January 21, 2015 from <<http://www.gebco.net>>.
- GraphPad, 1995–2014. How the AICc computations work. Retrieved January 21, 2015, from <[http://www.graphpad.com/guides/prism/6/curve-fitting/index.htm?reg\\_how\\_the\\_aicc\\_computations\\_work.htm](http://www.graphpad.com/guides/prism/6/curve-fitting/index.htm?reg_how_the_aicc_computations_work.htm)>.
- Hayes, G., Rivera, L., Kanamori, H., 2009. Source inversion of the W-phase: real-time implementation and extension to low magnitudes. *Seismol. Res. Lett.* 80 (5), 817–822. <http://dx.doi.org/10.1785/gssrl.80.5.817>.
- Ji, C., Helmberger, D.V., Wald, D.J., 2004. A teleseismic study of the 2002 Denali fault, Alaska, earthquake and implications for rapid strong-motion estimation. *Earthquake Spectra* 20 (3), 617–637. <http://dx.doi.org/10.1193/1.1778388>.
- Jolivet, R., Duputel, Z., Riel, B., Simons, M., Rivera, L., Minson, S.E., Fielding, E.J., 2014. The 2013 M<sub>w</sub> 7.7 Balochistan earthquake: seismic potential of an accretionary wedge. *Bull. Seismol. Soc. Am.* 104 (2), 1020–1030. <http://dx.doi.org/10.1785/0120130313>.
- Kanamori, H., Rivera, L., 2008. Source inversion of W phase: speeding up seismic tsunami warning. *Geophys. J. Int.* 175, 222–238. <http://dx.doi.org/10.1111/j.1365-246X.2008.03887.x>.
- Lay, T., Kanamori, H., Ammon, C.J., Hutko, A.R., Furlong, K., Rivera, L., 2009. The 2006–2007 Kuril Islands great earthquake sequence. *J. Geophys. Res. Solid Earth* (1978–2012) 114 (B11). <http://dx.doi.org/10.1029/2008JB006280>.
- Lay, T., Ammon, C.J., Hutko, A.R., Kanamori, H., 2010a. Effects of kinematic constraints on teleseismic finite-source rupture inversions: Great Peruvian earthquakes of 23 June 2001 and 15 August 2007. *Bull. Seismol. Soc. Am.* 100 (3), 969–994. <http://dx.doi.org/10.1785/0120090274>.
- Lay, T., Ammon, C., Kanamori, H., Rivera, L., Koper, K., Hutko, A., 2010b. The Samoa-Tonga great earthquake triggered doublet. *Nature* 466 (2010b), 964–968. <http://dx.doi.org/10.1038/nature09214>.
- Lay, T., Ye, L., Kanamori, H., Yamazaki, Y., Cheung, K.F., Kwong, K., Koper, K.D., 2013a. The October 28, 2012 M<sub>w</sub> 7.8 Haida Gwaii underthrusting earthquake and tsunami: slip partitioning along the Queen Charlotte Fault transpressional plate boundary. *Earth Planet. Sci. Lett.* 375, 57–70. <http://dx.doi.org/10.1016/j.epsl.2013.05.005>.
- Lay, T., Duputel, Z., Ye, L., Kanamori, H., 2013b. The December 7, 2012 Japan Trench intraplate doublet (M<sub>w</sub> 7.2, 7.1) and interactions between near-trench intraplate thrust and normal faulting. *Phys. Earth Planet. Inter.* 220, 73–78. <http://dx.doi.org/10.1016/j.pepi.2013.04.009>.
- Meng, L., Ampuero, J.P., Stock, J., Duputel, Z., Luo, Y., Tsai, V.C., 2012. Earthquake in a maze: compressional rupture branching during the 2012 M<sub>w</sub> 8.6 Sumatra earthquake. *Science* 337 (6095), 724–726. <http://dx.doi.org/10.1126/science.1224030>.
- Nakamura, T., Tsuoboi, S., Kaneda, Y., Yamanaka, Y., 2010. Rupture process of the 2008 Wenchuan, China earthquake inferred from teleseismic waveform inversion and forward modeling of broadband seismic waves. *Tectonophysics* 491 (1), 72–84. <http://dx.doi.org/10.1016/j.tecto.2009.09.020>.

- Oglesby, D.D., Dreger, D.S., Harris, R.A., Ratchkovski, N., Hansen, R., 2004. Inverse kinematic and forward dynamic models of the 2002 Denali fault earthquake, Alaska. Bull. Seismol. Soc. Am. 94 (6B), S214–S233. <http://dx.doi.org/10.1785/0120040620>.
- Park, J., Song, T.R.A., Tromp, J., Okal, E., Stein, S., Roult, G., Rosat, S., 2005. Earth's free oscillations excited by the 26 December 2004 Sumatra-Andaman earthquake. Science 308 (5725), 1139–1144. <http://dx.doi.org/10.1126/science.1112305>.
- Robinson, D.P., Henry, C., Das, S., Woodhouse, J.H., 2001. Simultaneous rupture along two conjugate planes of the Wharton Basin earthquake. Science 292 (5519), 1145–1148. <http://dx.doi.org/10.1126/science.1059395>.
- Stein, S., Okal, E.A., 2005. Seismology: speed and size of the Sumatra earthquake. Nature 434 (7033), 581–582. <http://dx.doi.org/10.1038/434581a>.
- Tsai, V., Nettles, M., Ekström, G., Dziewonski, A.M., 2005. Multiple CMT source analysis of the 2004 Sumatra earthquake. Geophys. Res. Lett. 32. <http://dx.doi.org/10.1029/2005GL023813>.
- USGS, 2000, June. M7.9 – southern Sumatra, Indonesia. Retrieved September 2, 2015, from <[http://earthquake.usgs.gov/earthquakes/eventpage/usp0009txv#scientific\\_finitefault](http://earthquake.usgs.gov/earthquakes/eventpage/usp0009txv#scientific_finitefault)>.
- USGS, 2001, January. M7.7 – Gujarat, India. Retrieved September 4, 2015, from <[http://earthquake.usgs.gov/earthquakes/eventpage/usp000a8ds#scientific\\_finitefault](http://earthquake.usgs.gov/earthquakes/eventpage/usp000a8ds#scientific_finitefault)>.
- USGS, 2002, November. The 2002 Denali Fault earthquake. Retrieved February 1, 2015, from <<http://earthquake.usgs.gov/eqcenter/eqinthenews/2002/uslbl/reports/index.php>>.
- USGS, 2002, October. M7.6 – near the north coast of Papua, Indonesia. Retrieved February 1, 2015 from <[http://earthquake.usgs.gov/earthquakes/eventpage/usp000be54#scientific\\_finitefault](http://earthquake.usgs.gov/earthquakes/eventpage/usp000be54#scientific_finitefault)>.
- USGS, 2005, September. M7.6 – New Ireland region, Papua New Guinea. Retrieved September 11, 2015 from <[http://earthquake.usgs.gov/earthquakes/eventpage/usp000dz2j#scientific\\_finitefault](http://earthquake.usgs.gov/earthquakes/eventpage/usp000dz2j#scientific_finitefault)>.
- USGS, 2009, September. M8.1-Samoa Islands region (BETA) 2009-09-29 17:48:10 UTC. Retrieved January 21, 2015 from <[http://earthquake.usgs.gov/earthquakes/eqinthenews/2009/us2009mdbi/finite\\_fault.php](http://earthquake.usgs.gov/earthquakes/eqinthenews/2009/us2009mdbi/finite_fault.php)>.
- USGS, 2009, August. M7.5 – Andaman Islands, India region. Retrieved September 4, 2015 from <[http://earthquake.usgs.gov/earthquakes/eventpage/usp000h05x#scientific\\_finitefault](http://earthquake.usgs.gov/earthquakes/eventpage/usp000h05x#scientific_finitefault)>.
- USGS, 2012, October. M7.8 – Haida Gwaii, Canada. Retrieved January 21, 2015 from <[http://earthquake.usgs.gov/earthquakes/eventpage/usp000juhz#scientific\\_finitefault:us\\_usp000juhz](http://earthquake.usgs.gov/earthquakes/eventpage/usp000juhz#scientific_finitefault:us_usp000juhz)>.
- USGS, 2013, September. M7.7 – 61km NNE of Awaran, Pakistan. Retrieved February 1, 2015 from <[http://earthquake.usgs.gov/earthquakes/eventpage/usb000jyiv#scientific\\_finitefault](http://earthquake.usgs.gov/earthquakes/eventpage/usb000jyiv#scientific_finitefault)>.
- USGS, 2014, April. M7.5-70km SW of Panguna, Papua New Guinea. Retrieved January 21, 2015 from <[http://earthquake.usgs.gov/earthquakes/eventpage/usb000pr89#scientific\\_finitefault](http://earthquake.usgs.gov/earthquakes/eventpage/usb000pr89#scientific_finitefault)>.
- USGS, 2014b, April. M7.6 – 93km SSE of Kirakira, Solomon Islands. Retrieved January 21, 2015 from <[http://earthquake.usgs.gov/earthquakes/eventpage/usc000phx5#scientific\\_finitefault](http://earthquake.usgs.gov/earthquakes/eventpage/usc000phx5#scientific_finitefault)>.
- Vallée, M., Satriano, C., 2014. Ten year recurrence time between two major earthquakes affecting the same fault segment. Geophys. Res. Lett. 41 (7), 2312–2318. <http://dx.doi.org/10.1002/2014GL059465>.
- Wessel, P., Smith, W.H.F., 1991. Free software helps map and display data. EOS Trans. AGU 72 (441), 445–446.
- Ye, L., Lay, T., Koper, K.D., Smalley, R., Rivera, L., Bevis, M.G., Teferle, F.N., 2014. Complementary slip distributions of the August 4, 2003  $M_w$  7.6 and November 17, 2013  $M_w$  7.8 South Scotia Ridge earthquakes. Earth Planet. Sci. Lett. 401, 215–226. <http://dx.doi.org/10.1016/j.epsl.2014.06.007>.
- Zhan, Z., Kanamori, H., Tsai, V.C., Helmberger, D.V., Wei, S., 2014. Rupture complexity of the 1994 Bolivia and 2013 Sea of Okhotsk deep earthquakes. Earth Planet. Sci. Lett. 385, 89–96.
- Zinke, R., Hollingsworth, J., Dolan, J.F., 2014. Surface slip and off-fault deformation patterns in the 2013  $M_w$  7.7 Balochistan, Pakistan earthquake: implications for controls on the distribution of near-surface coseismic slip. Geochem. Geophys. Geosyst. 15 (12), 5034–5050.